Climatic and tectonic drivers of late Oligocene Antarctic ice volume

B. Duncan[1], R. McKay[1], R. Levy[1,2], T. Naish[1], J. Prebble[2], F. Sangiorgi[3], S. Krishnan[4,5], F. Hoem[3], C. Clowes[2], T. Dunkley Jones[6], E. Gasson[7], C. Kraus[1,8], D. K. Kulhanek[9,10] S. Meyers[11], H. Moossen[6,12], C. Warren[4], V. Willmott[13,14], G.T. Ventura[2,15] & J. Bendle[6]

[1] Antarctic Research Centre, Victoria University of Wellington, Wellington, 6140, New Zealand

[2] Geological and Nuclear Sciences, P.O. Box 30-368, Lower Hutt 5040, New Zealand

[3] Department of Earth Sciences, Marine Palynology and Paleoceanography, Department of Earth Sciences, Utrecht University, Princetonlaan 8a, 3584CB Utrecht, the Netherlands

[4] The Department of Earth and Planetary Sciences, Yale University, New Haven, CT 06211, USA

[5] Present address: CICERO Center for International Climate and Environmental Research, Oslo, Norway

[6] School of Geography, Earth and Environmental Sciences, University of Birmingham, Edgbaston, Birmingham, B15 2TT, UK

[7] University of Exeter, Penryn, Cornwall, TR10 9FE, UK

[8] Present address: Beca Ltd., P.O. Box 3942, Wellington, 6140, New Zealand.

[9] International Ocean Discovery Program, Texas A&M University, College Station, TX, USA

[10] Present address: Institute of Geosciences, Christian-Albrechts-University of Kiel, 24118, Kiel, Germany

[11] Department of Geoscience, University of Wisconsin-Madison, Madison, WI, USA

[12] Present address: Max Planck Institute for Biogeochemistry, P.O. Box 10 01 64, 07701 Jena, Germany

[13] NIOZ Royal Netherlands Institute for Sea Research, Department of Marine Organic Biogeochemistry, P.O. Box 59, 1790 AB Den Burg (Texel), The Netherlands

[14] Present address: International Cooperation Unit, Alfred Wegener Institute, 27570, Bremerhaven, Germany

[15] Present address: Department of Geology, Saint Mary's University, 923 Robie Street, Halifax, Nova Scotia, B3H 3C3, Canada

Correspondence to: Bella J. Duncan (Bella.Duncan@vuw.ac.nz)

Long-term changes in radiative forcings (CO_2, orbital variations) are thought to be the primary driver of the Cenozoic evolution of the Antarctic Ice Sheets (AIS), but the tectonic evolution of Antarctica may also have played a substantive role. Deep-sea foraminiferal oxygen isotope records ($\delta^{18}O$) provide a combined measure of global continental ice volume and ocean temperature, but do not provide direct insights on non-radiative influences on AIS dynamics. Here, we generate the first Antarctic-proximal (Ross Sea and Wilkes Land) Cenozoic compilation of upper ocean temperature, and find that trends of ocean temperature, atmospheric CO_2 and $\delta^{18}O$ do largely co-vary. However, this relationship is less clear for the late Oligocene, when high latitude cooling occurred, despite $\delta^{18}O$ values implying global warming and ice volume loss. We propose West Antarctic Ice Sheet retreat occurred in response to a tectonically-driven marine transgression at this time, with warm surface waters precluding marine-based ice sheet growth. Marine-based ice sheet expansion only occurred when ocean temperatures cooled enough during cold orbits and low atmospheric CO_2 at the Oligocene-Miocene transition. Our results support hypotheses of a threshold response to atmospheric CO_2, below which Antarctica's marine ice sheets grow, and above which ocean warming exacerbates their retreat.

It is well-known that the AIS is sensitive to multi-millennial scale variations in Earth's astronomical configuration[1–4]. However, million-year timescale trends in AIS volume are generally controlled by more gradual changes in greenhouse gas concentrations[5], changing continental configurations modulating heat flow towards Antarctica[6], and topographic changes driven by subsidence and erosion on the continent[7,8]. Benthic deep sea $\delta^{18}O$ records provide critical insights into Cenozoic climate variability[3,9], but are a signal of both deep ocean temperature and global ice volume change, and

64 additional information from Antarctic-proximal archives are required to fully understand the controls
65 on past AIS dynamics.
66
67 Models and near-field geological data indicate the AIS in the Ross Sea region is sensitive to climate
68 forcings such as local insolation, ocean heat flux and local sea level changes, and records variability of
69 both the East (EAIS) and West Antarctic Ice Sheets (WAIS)[1,10–12]. Millions of years of erosion,
70 sedimentation, thermal subsidence and tectonic rifting in the Ross Sea[7,8] have resulted in West
71 Antarctica evolving from an elevated and subaerial region capable of sustaining a large terrestrial ice
72 sheet in the Oligocene[13], to the present day over-deepened, subsided continental shelf bathymetry
73 occupied by marine-based ice sheets (Fig. 2a)[7,14,15].
74
75 Here, we investigate the role of climatic and non-climatic drivers on long-term AIS variability by
76 examining the relationship between high-latitude temperature, atmospheric CO_2 and ice volume. We
77 hypothesize that if AIS volume changes were driven directly by radiative forcing and related ocean
78 temperatures, then Southern Ocean sea surface temperatures (SST) should largely covary with
79 atmospheric CO_2 and benthic $\delta^{18}O$ records. To test this, we reconstruct Cenozoic upper ocean
80 temperatures in the Ross Sea and Wilkes Land margin region from a compilation of sediment and
81 outcrop samples (Fig. 1) using glycerol dialkyl glycerol tetraethers (GDGTs), membrane lipids formed
82 by archaea and some bacteria[16] (Supplementary Information S1). We apply the recently developed
83 OPTiMAL machine learning-based temperature calibration to new and legacy GDGT datasets to assign
84 SST estimates (average standard deviation is 3.61°C)[17]. We compare these to other GDGT-based

temperature calibrations and temperature estimates from fossil assemblages and other geochemical datasets at high southern latitudes (Supplementary Information S1 and Supplementary Table S1). Compiling a long-term Cenozoic Antarctic proximal temperature record necessitates the use of multiple core sites across a complex glacimarine continental shelf to rise depositional transect, influenced by changing water masses and the proximity of ocean fronts. This is particularly the case for Integrated Ocean Drilling Program (IODP) Site U1356 on the Wilkes Land continental rise. This site is proximal to the southern boundary the Antarctic Circumpolar Current (ACC) where glacial-interglacial (G-I) scale variability is influenced by frontal migration[18,19] (Fig. 1), compared to sites located >14º of latitude further south in the Ross Sea (Fig. 1). These caveats are discussed in more detail in Supplementary Information S2.

Cenozoic SST compilation

Mid-Eocene (~48-38 Ma) Ross Sea glacial erratics, eroded from subglacial strata and deposited during subsequent ice sheet advances (Fig. 1; Methods; paleolatitude of ~80°S) display highly variable OPTiMAL SSTs (average ~10 °C; maximum values reaching 20 °C), likely reflecting a range of climate states and/or depositional environments over a wide time range (Fig. 2d)[20]. Such values are consistent with temperate terrestrial palynomorph assemblages, shark teeth, mollusc assemblages and a probable crocodile tooth (Supplementary Table 1). Mid and upper Eocene SSTs in the CIROS-1 drill core (Fig. 1, Extended Data Fig. 1) indicate Ross Sea temperatures were 4-6.5 °C by ~36 Ma (Fig. 2), consistent with a range of qualitative indicators of Southern Ocean cooling and ice growth ~2 million years prior to widespread AIS expansion across the Eocene Oligocene Transition (EOT; 34 Ma)

106 (Supplementary Table 1)[21,22]. During the EOT (Fig. 2), Ross Sea SSTs dropped to as low as 2.4 °C,
107 comparative with mid- to high-latitude Southern Ocean cooling of ~5 °C[23]. By the early Oligocene,
108 SSTs warmed again, reaching similar values to the late Eocene (~4-6 °C) (Fig. 2), a warming also
109 observed at the Wilkes Land margin (Site U1356; Fig. 1). However, at this more northern site
110 (paleolatitude of ~59°S) SSTs were significantly warmer (reaching 15-20 °C), with a ~10-15 °C
111 temperature gradient reflecting the ~14 degrees latitudinal offset (~1650 km) between sites in our
112 compilation, as well as warmer lower-latitude water masses bathing the Wilkes Land margin prior to
113 Tasmanian Gateway widening[18].
114
115 A substantial latitudinal temperature gradient persisted throughout the Oligocene, although both regions
116 experienced cooling at ~25 Ma (Fig. 2 and 3). Following the Oligocene-Miocene Transition (OMT; ~23
117 Ma), Ross Sea SSTs in the early Miocene averaged 3 °C (standard deviation of 1.5°C), with variability
118 likely driven by astronomically-paced climate cycles. GDGT-based SSTs in the Ross Sea during the
119 Miocene Climate Optimum (MCO; ~17-15 Ma) average 2.2 °C (standard deviation of 1.5°C). However,
120 warmer values up to 6-8 °C occur during peak MCO warmth (Fig. 2)[11], comparable with estimates from
121 carbonate clumped isotope (Δ_{47}) analysis and leaf wax isotopes in AND-2A cores (Fig. 1)[11,24], and
122 vegetation assemblages in Transantarctic Mountain lake sediments[25] (Supplementary Table S1). Wilkes
123 Land SSTs remained warmer than the Ross Sea, averaging 7.5 °C, with a larger standard deviation of
124 3.6 °C (Fig. 2) attributed to warm-water incursions due to weakened Southern Ocean frontal systems
125 that influence Site U1356[19]. The middle Miocene Climate Transition (MMCT, ~14.6-13.8 Ma) is
126 characterised by Ross Sea SSTs averaging ~2.5 °C, but not exceeding 5 °C, although only five samples

were examined due to extensive erosion from continental shelf-wide ice-sheet grounding events limiting availability of datable stratigraphic material[11,15]. Across the MMCT, surface cooling and decreasing temperature gradients between Wilkes Land and the Ross Sea likely reflects intensification or southward migration of the Antarctic Divergence proximal to Site U1356 (Fig. 2). Early Pliocene Ross Sea GDGT-based SSTs derived from AND-1B (Fig. 1) averaged ~6°C, consistent with diatom assemblages and evidence of limited summer sea ice during peak interglacials of the early Pliocene[26] . Such surface temperatures are consistent with mid-Pliocene global mean annual SST reconstructions of 2-3 °C above pre-industrial, assuming 2-3x polar amplification[27]. The return to warm values similar to the Oligocene and MCO seems surprising at face value, but AND-1B is inherently biased toward interglacial values (Supplementary Information S2). In addition, the warmest temperatures in AND-1B occur during the transitions into and out of the peak interglacial intervals, when sedimentary facies and geochemical proxies indicate enhanced glacial meltwater processes and seasonal sea ice melt, which acts to enhance thermal stratification and warm upper ocean temperatures[26]. Cold temperatures of 1-3°C predominantly characterised the late Pliocene-Pleistocene in the Ross Sea (Fig. 2).

Late Oligocene ice sheet retreat in a cooling climate

Our 46 million-year Ross Sea temperature record shows a trend of ocean cooling in concert with declining atmospheric CO_2 and increasing benthic foraminiferal $\delta^{18}O$ values[3,28,29], implying high latitude temperature and ice volume are largely coupled over the Cenozoic (Fig. 2). However, this relationship is notably weaker during the late Oligocene (Fig. 3). Following a positive isotope excursion at ~27 Ma (Oi2b event), average $\delta^{18}O$ values then decrease by -0.4 to -0.6 ‰ over a ~3 million year

148 period, a trend widely interpreted as an interval of prolonged global warming[9]. Evidence of circum-
149 Antarctic warm conditions between 27 and 25 Ma include (i) warm-water nannofossil assemblages over
150 Maud Rise and the Kerguelen Plateau[30], (ii) Ross Sea dinocyst assemblages and TEX_{86}-based SSTs
151 (DSDP Site 274)[31], and (iii) dinocyst and sedimentary evidence of limited sea ice and ice-rafted debris
152 from offshore Wilkes Land[32,33]. In the Ross Sea, late Oligocene surface water temperature data are
153 lacking prior to 25.5 Ma in DSDP Site 270, with samples between 25.5-25 Ma recording relatively
154 warm SSTs (~6-7°C) and diverse foraminifera assemblages with more temperate affinities compared to
155 younger Oligocene assemblages[34].
156
157 After ~25 Ma, the deep sea $\delta^{18}O$ record continues to trend towards lower values, implying warming
158 (Fig. 3), yet our temperature reconstructions show ocean surface cooling in the Ross Sea and Wilkes
159 Land. Paleoenvironmental proxies also suggest SST cooling and sea ice cover at this time in the Ross
160 Sea, including nannofossil, marine palynomorph, and marine macrofossil assemblages in uppermost
161 Oligocene sediments from Cape Roberts Project (CRP)[35] (Supplementary Table 1). Sedimentary facies
162 analysis, and chemical weathering indicators in the CRP and CIROS-1 cores also suggest a minimal
163 change or a long-term cooling trend during the late Oligocene, with conditions periodically cold enough
164 to allow for orbitally-paced marine-based EAIS outlet glacier advance into the western Ross Sea
165 (Supplementary Table 1)[4]. Seismic disconformities also indicate Wilkes Land continental shelf marine-
166 based ice advance also occurred after ~25 Ma, and are associated with mass transport deposits on the
167 continental rise at IODP Site U1356[33] (Supplementary Table 1).
168

169 The contrast of a cooling Antarctic climate from ~25 Ma with inferred warming and/or ice volume
170 decrease from deep sea $\delta^{18}O$ records has previously been attributed to reduced proto Antarctic Bottom
171 Water formation, and increased warmer, Northern Hemisphere-sourced deep waters influencing drill
172 sites north of the ACC[36,37]. While this may explain the latitudinal $\delta^{18}O$ gradient, it does not fully explain
173 the trend to lower $\delta^{18}O$ values (reaching a minima at ~24 Ma) in both the Pacific and Atlantic oceans
174 (Fig. 3), especially if the precursor surface waters that form Antarctic Bottom Water in the Ross Sea are
175 cooling as our SST compilation implies. There is also considerable heterogeneity in global SST records
176 over this time[38], with high southern latitudes (discussed here) and equatorial Atlantic records suggesting
177 warming peaked between 26 and 25 Ma, while North and Southwestern Atlantic records show
178 continued warming until 24-23.5Ma[38]. In the context of these records, we present a hypothesis that
179 reconciles evidence of Antarctic cooling on a background of subsidence-driven ice sheet retreat in West
180 Antarctica, that we argue provides a mechanism to explain the observed trends in global ocean $\delta^{18}O$ and
181 globally distributed ocean temperature records for the Late Oligocene[37,38].
182
183 Ice sheet modelling studies that use restored Antarctic paleotopographies show a largely subaerial West
184 Antarctica in the Oligocene could accommodate a much larger reservoir of terrestrial ice than today,
185 even with warmer-than-present ocean temperatures in the Ross Sea[7,8,39,40]. Marine-based ice is
186 inherently more sensitive to ocean warming, and retreat is exacerbated by non-linear processes[39–41]. We
187 suggest that a transgression of relatively warm water across West Antarctica due to tectonic subsidence
188 and glacial erosion drove ocean-induced retreat of the terrestrial WAIS, resulting in a gradual and
189 progressive decrease in ice extent and volume in warmer-than-present late Oligocene climates. The

190 evidence for regional tectonic subsidence comes from a dense network of seismic reflector correlations
191 to DSDP Site 270, for which age control and paleodepth reconstructions show an extended episode of
192 late Oligocene deepening of the sea-floor between ~26 Ma and the early Miocene[7,15,34,42] (Fig. 3).
193 Terrestrial to shallow marine sediments at the base of DSDP site 270 are overlain by mudstones with
194 benthic foraminiferal assemblages indicating water depths of ~200 m between 25.5-24.8 Ma, deepening
195 to ~500 m by ~24.5 Ma, with ongoing subsidence continuing after this time (Fig. 3). As the mid-Ross
196 Sea paleocontinental shelf subsided below sea level, and despite cooling of local SSTs, ocean
197 temperatures remained too warm (Fig. 3) for significant marine-based ice development, driving a long-
198 term decrease in Antarctic ice volume and contributing to the decreasing trend in global benthic $\delta^{18}O$.
199
200 Model experiments show that under constant atmospheric CO_2 concentrations of 500 ppm, changes in
201 bed elevation alone between EOT and OMT topographies can account for an ice volume difference of
202 $5.7x10^6$ km^3 using the 'median' reconstruction of ref. [8] (see Methods). Interestingly, a larger, terrestrial
203 WAIS serves to buttress and increase the size of the EAIS, and subsidence-driven retreat in the Ross
204 Sea would also lead to a significant loss of the inland EAIS[43]. If most of the subsidence between the
205 EOT and OMT occurred in the late Oligocene, as indicated by seismic data and the DSDP site 270
206 reconstructions, then subsidence could account for ice loss equating to an average $\delta^{18}O$ shift of -0.2 ‰
207 (see methods)[39]. However, this example was performed under constant climate state, feedbacks in the
208 earth system or orbitally driven climate changes over long-time periods are not accounted for in this
209 estimate. The total $\delta^{18}O$ decrease from Oi2b at 26.7 Ma to 24 Ma is on the order of -0.4 to -0.6 ‰, and
210 it is likely that the earliest phase of this signal was indeed amplified by climate-driven retreat following

211 the warming out of the ~27 Ma Oi2b glacial event[18] . However, following the initiation of cooling in our
212 compilation at ~25 Ma, $\delta^{18}O$ declines by a further ~0.05-0.2 ‰ (Fig. 3a), which is consistent with
213 continued long term tectonic-driven retreat. As noted earlier, this signal has previously been explained
214 by heterogeneity in deep water temperature signals[36,37] and indeed tectonically-driven Late Oligocene
215 marine AIS retreat could have driven this heterogeneity. Models for the Pliocene show AIS loss in West
216 Antarctica and Wilkes Land acts to slow the ACC and Pacific Ocean overturning circulation - leading to
217 reduced AABW formation, increased heat transport to the North Atlantic, and divergence of global deep
218 water mass temperatures in the Pacific and Atlantic ocean[44]. Shifts in ACC circulation and zonal winds
219 relating to contracted AIS volume could also shift surface water connectivity between the ocean basins,
220 and wind-driven upwelling systems[26], contributing to the significant heterogeneity in global surface
221 water trends through this time[38].
222
223 In summary, we suggest that a continuous decline in average ice sheet volume occurred between ~27-24
224 Ma. This was likely driven initially by the shift to warmer climatic conditions following the 27 Ma Oi2b
225 glacial event[18], but despite subsequent cooling from ~25 Ma in the Ross Sea and Wilkes Land, the
226 marine sectors of AIS continued to retreat due to basin subsidence and marine incursion across West
227 Antarctica (Fig. 3). Ross Sea SSTs had cooled to ~3 °C by 24.5 Ma, coinciding with a 1.2 Myr node in
228 obliquity, an astronomical configuration favourable to ice sheet expansion[2]. Proximal glacimarine
229 sedimentary facies were deposited at DSDP site 270 at this time and mark a period of ice sheet
230 grounding line advance into the Ross Sea (Fig. 3)[42,45]. A major increase in obliquity sensitivity (S_{obl}) is
231 also observed at ~24.5 Ma, a metric associated with marine ice sheet advance and enhanced AIS and

ocean connectivity (Fig. 3)[45]. Atmospheric CO_2 records through the Oligocene are sparse and there is still considerable uncertainty surrounding the absolute values assigned to individual data points, but a clear decline in CO_2 values occurs between the early and late Oligocene (Fig. 2)[5,46]. Pleistocene to Pliocene-based model-data comparisons[1,8,41] suggest values much lower than 400 ppm (e.g. ~280 ppm) are required for marine ice sheet advance onto the mid-continental shelf of the Ross Sea, while above 400 ppm marine-based ice is absent from West Antarctica, and sectors of East Antarctica[41]. Higher-resolution atmospheric proxy CO_2 records, alongside further validation of absolute values, in this critical interval would allow for a better understanding of these thresholds. However, the episode of marine ice sheet advance at 24.5 Ma was transient, and relatively muted in scale in the $\delta^{18}O$ record. Following this, a trend towards a smaller WAIS is reflected by deeper water, ice distal facies in the latest Oligocene in DSDP site 270 (Fig. 3)[34,42] and the continued decrease in average deep sea $\delta^{18}O$ until 24 Ma.

After 24 Ma, Ross Sea SSTs continued to cool, crossing a threshold to enable marine-based ice sheets to migrate across the deep continental shelf (Fig. 3). This culminated in the Mi-1 glaciation at 23 Ma, which peaked during a 400 kyr eccentricity minimum and a 1.2 Myr node in obliquity, an optimal configuration for ice growth due to extended low seasonality and cool summer temperatures[2]. Some proxy atmospheric CO_2 reconstructions suggests values reached as low as 265 ppm ($2\sigma_{-111}^{+166}\ ppm$) during Mi-1[47]. The Mi-1 event is associated with regional seismic unconformities[15], and major disconformities in DSDP site 270[42] and CRP-2/2A[4], while $\delta^{18}O$ records indicate it lasted ~200-300 kyrs before rebounding in the earliest Miocene towards late Oligocene values. This is consistent with a rapid

253 increase in atmospheric CO_2[47], an astronomical configuration favouring warming, and marine-based ice
254 sheet retreat over the subsided Ross Sea continental shelf. Between 17.8-17.4 Ma, SSTs of ~1.5-3.4°C
255 at AND-2A indicate the threshold for marine-based WAIS advance was again crossed, as evidenced by
256 recent provenance studies from IODP Site U1521 indicating a large WAIS advance resulted in further
257 lowering of elevations in the interior of West Antarctic via glacial erosion[43].
258
259 Our compilation of proximal Antarctic temperatures provide climatic constraints on the late Oligocene
260 expansion of marine-based ice sheets, on the background of competing influences on AIS volume
261 resulting from crustal subsidence in West Antarctica. These results are consistent with the concept of a
262 threshold response suggested by previous studies to occur at atmospheric CO_2 values of ~400
263 ppm[1,10,11,45], above which ocean warming at Antarctica's margin greatly exacerbates marine ice sheet
264 retreat into interior subglacial basins, with profound consequences for global sea level.
265
266
267
268

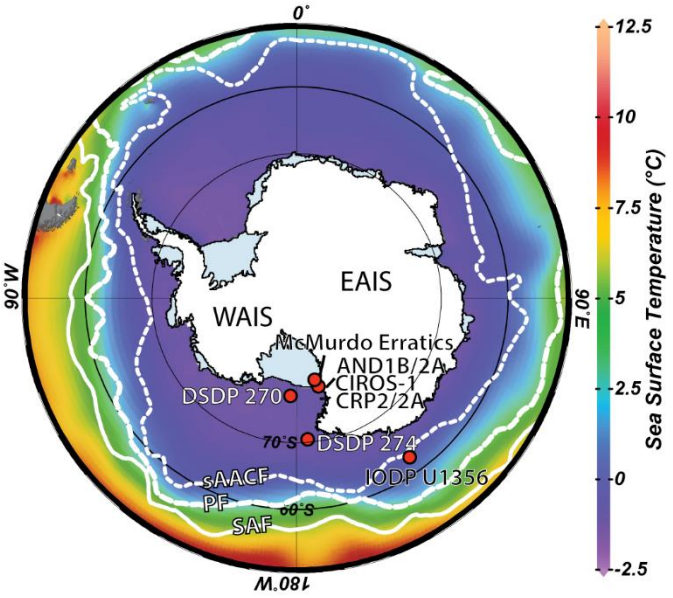

269

270 *Figure 1: Location Map of the drill core and sample locations used in this study. Annual sea surface*

271 *temperatures*[48] *and positions of the southern Antarctic Circumpolar Current Front (sAACF), Antarctic*

272 *Polar Front (APF) and Subantarctic Front (SAF)*[49]*. WAIS- West Antarctic Ice Sheet, EAIS- East*

273 *Antarctic Ice Sheet. Plotted using Ocean Data Viewer (https://odv.awi.de).*

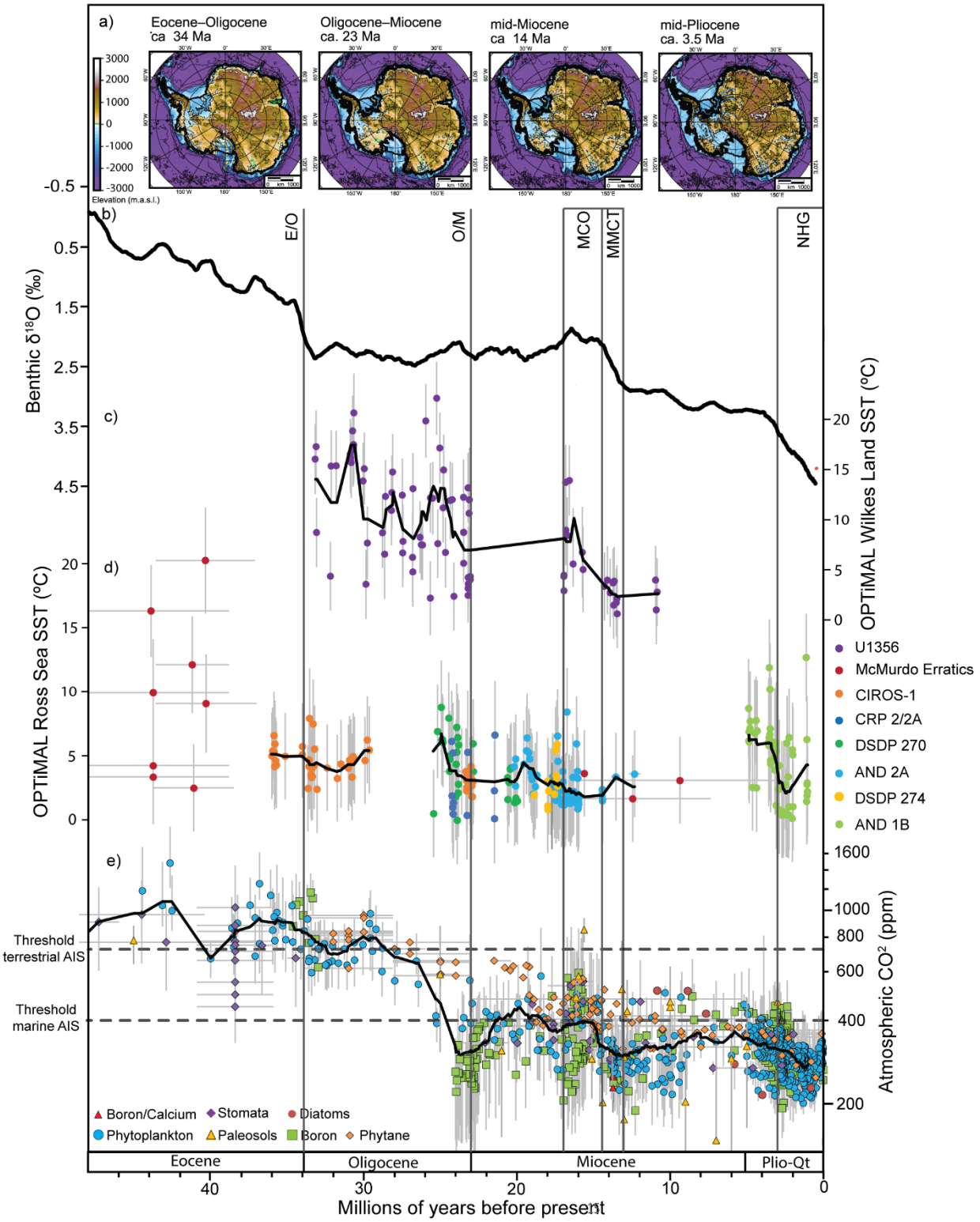
a)
Eocene–Oligocene
ca 34 Ma
Oligocene–Miocene
ca. 23 Ma
mid-Miocene
ca 14 Ma
mid-Pliocene
ca. 3.5 Ma
Elevation (m.a.s.l.)
b)
c)
d)
e)
E/O
O/M
MCO
MMCT
NHG
Benthic δ18O (‰)
OPTiMAL Ross Sea SST (°C)
OPTiMAL Wilkes Land SST (°C)
Atmospheric CO2 (ppm)
U1356
McMurdo Erratics
CIROS-1
CRP 2/2A
DSDP 270
AND 2A
DSDP 274
AND 1B
Threshold terrestrial AIS
Threshold marine AIS
Boron/Calcium
Stomata
Diatoms
Phytoplankton
Paleosols
Boron
Phytane
Eocene
Oligocene
Miocene
Plio-Qt
Millions of years before present

274

Figure 2. Sea surface temperature compilation from Ross Sea and Wilkes Land sample sites. a) Topographic reconstructions from Paxman et al., 2019. b) 1 Myr moving average of benthic $\delta^{18}O$ stack[3]*. c) OPTiMAL SSTs for site U1356 Wilkes Land have been recalibrated based on GDGT abundances reported previously*[18,19]*, with vertical error bars representing the standard deviation of the temperature estimate (1σ). Samples with nearest neighbour values above 0.5 and samples from mass transport deposits have been removed from the compilation. The black line represents a 1 Myr moving average d) OPTiMAL SSTs for Ross Sea sample sites, with vertical error bars representing the standard deviation of the temperature estimate (1σ). Samples with nearest neighbour values above 0.5 have been removed from the compilation. The black line represents a 1 Myr moving average. e) Atmospheric CO_2 concentrations, with the black line representing a 2 Myr moving average, (see methods). Dashed horizontal bars represent atmospheric CO_2 thresholds for a terrestrial AIS*[21]*, and marine AIS*[1]*. Vertical bars indicate significant climate events; E/O= Eocene/Oligocene boundary, O/M= Oligocene/Miocene boundary, MCO= Miocene Climate Optimum, MMCT= Middle Miocene Climate Transition, NHG= Northern Hemisphere glaciation.*

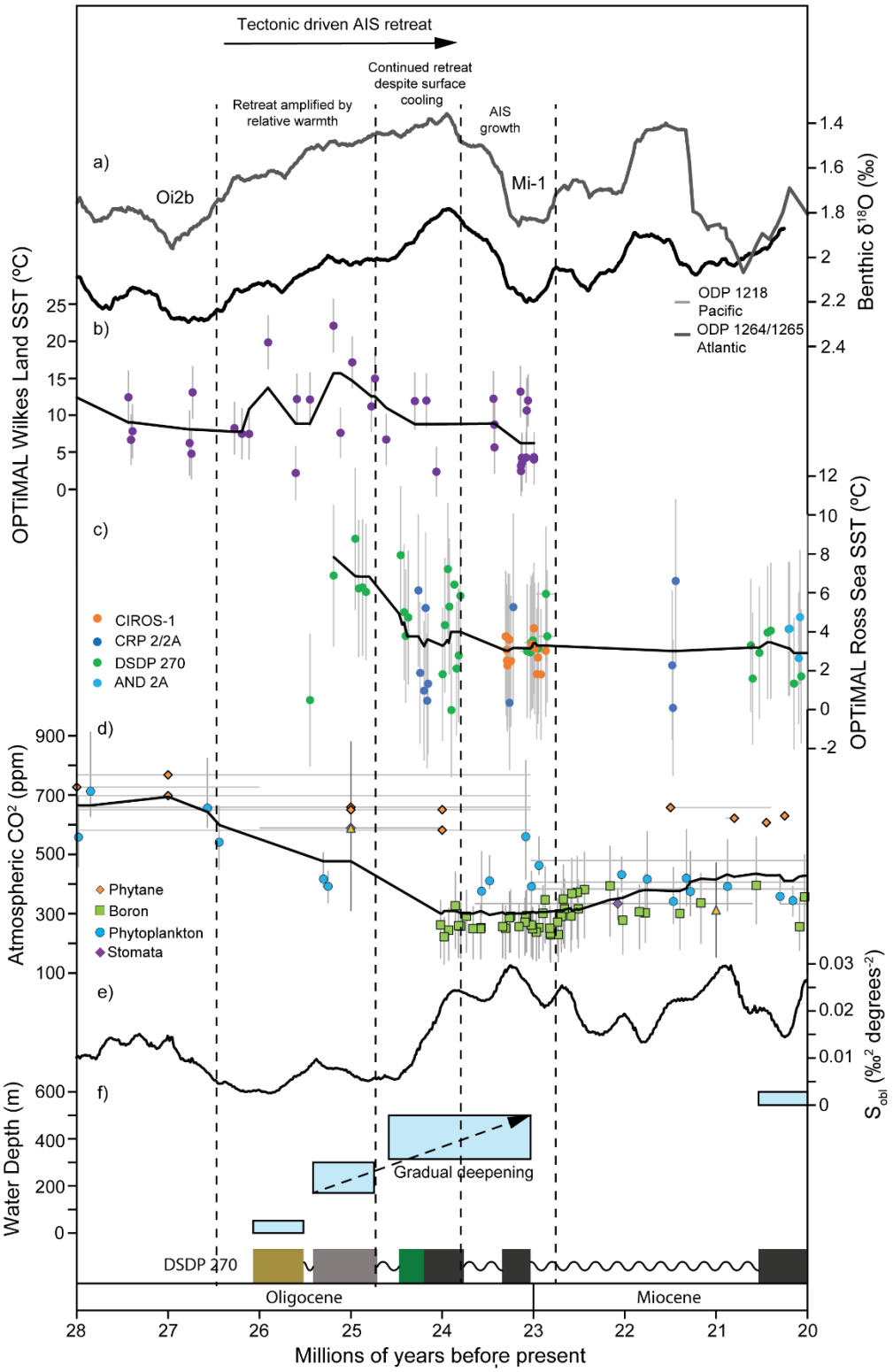
Tectonic driven AIS retreat
Retreat amplified by relative warmth
Continued retreat despite surface cooling
AIS growth
a)
Oi2b
Mi-1
ODP 1218 Pacific
ODP 1264/1265 Atlantic
Benthic δ18O (‰)
b)
OPTiMAL Wilkes Land SST (°C)
c)
CIROS-1
CRP 2/2A
DSDP 270
AND 2A
OPTiMAL Ross Sea SST (°C)
d)
Atmospheric CO2 (ppm)
Phytane
Boron
Phytoplankton
Stomata
e)
Sobl (‰2 degrees-2)
f)
Water Depth (m)
Gradual deepening
DSDP 270
Oligocene
Miocene
Millions of years before present

290

Figure 3. Late Oligocene- Early Miocene climate transition. a) 500 kyr moving averages of high resolution benthic $\delta^{18}O$ records for the late Oligocene from ODP 1218[2] *and ODP 1264/1265*[50]*. b) Wilkes Land OPTiMAL temperatures with a 500 kyr moving average in black. c) Ross Sea OPTiMAL temperatures with a 500 kyr moving average in black. d) Atmospheric CO_2 with a 1 myr moving average in black (see methods). e) Obliquity sensitivity*[45]*. f) DSDP 270 paleo water depth schematic*[42]*, with core log beneath. The light brown on the core log represents an estuarine, shallow marine depositional setting, light grey represents a deepening shelf setting, the green box signifies glacially derived diamictite, and dark grey colour represents an outer shelf to deeper marine setting.*

Methods

Sampling Sites and Age Models

Proximal Antarctic cores contain frequent unconformities, which is often the product of ice sheet overriding or other erosional processes in a glacimarine environment. In order to compile a long-term Cenozoic record of ocean temperatures from the Ross Sea, this has necessitated using multiple sampling sites and core sites from across the region (Fig. 1). We present data from the McMurdo Erratics, CIROS-1, DSDP 270, CRP-2A and DSDP 274, and compile this with previously published data from ANDRILL 1B and 2A. Age models have been developed using published age datums (Supplementary Data Table 3), but in order to ensure a consistent approach for assigning ages to core depths between datums, we use the Bayesian age-depth modelling functionality in the R package Bchron (Supplementary Data Table 3)[51]. The sites included in the Ross Sea compilation are detailed below. We

311 have compared our Ross Sea compilation to a previously published dataset from IODP U1356, offshore
312 the Wilkes Land margin, with GDGT abundances, age model and lithologies[18,33,52].

313 **McMurdo Erratics**

314 The oldest sediments used in this compilation are glacial erratics, collected from the Mount Discovery
315 and Minna Bluff region (Fig. 1)[53]. The erratics have been eroded from sediments deposited in sub-ice
316 basins in the western Ross Sea associated with early Cenozoic rifting during Gondwanaland breakup.
317 These rift-fill sediments were subsequently eroded (likely from the Discovery Deep region) and
318 transported to surficial morainal deposits by expanded ice sheets during past glacial periods. The
319 erratics sampled in this study were deposited in coastal-terrestrial and nearshore marine environments[53].
320 Ages for the erratics from the volumes in Harwood and Levy (2000)[53] have been updated to most recent
321 ages for the described taxa (Supplementary Data Table 2).

322 **CIROS-1**

323 The CIROS-1 core was drilled in McMurdo Sound in 1986 (Fig. 1)[54]. The upper part of the core (366-0
324 mbsf) is glacially influenced, with major glacial advances represented by massive and stratified
325 diamictites[55]. Below an unconformity, the lower sequence of the core (702-366 mbsf) displays
326 significantly less subglacial influence, containing marine mudstones and sandstones, but with ice rafted
327 debris indicating the presence of marine terminating glaciers at the coastline[55]. The upper part of the
328 core is late Oligocene/early Miocene in age[56]. Age control for the lower part of the CIROS-1 core has
329 undergone a series of revisions since recovery in 1986[57–59]. Our age model for the Eocene-Oligocene

boundary interval is an improvement on previous attempts, as we incorporate new observations of dinoflagellate cysts with occurrences recently described in other Antarctic and Southern Ocean cores[52,60–62]. These new observations allow precise constraint of the updated paleomagnetic record[59] of to the geomagnetic polarity timescale[63]. In addition, we include updated range data to constrain the ages of biostratigraphic events previously identified in the core. Microfossil reworking has long been recognised as a significant problem in the glacial sediments of Antarctica[64–66]. In constructing our age model, we have given preference to ensuring conformity to biostratigraphic first occurrences, and are much less concerned about apparent last occurrences in this setting. In addition to the biochronologic controls, we include new $^{87}Sr/^{86}Sr$ isotope ratio ages from disarticulated bivalves between 460 and 470 mbsf in the core. Measurements were undertaken at the CSIRO laboratory in Sydney. These ages are interpreted to represent minimum ages.

Biostratigraphic datums are shown in Supplementary Data Table 1, the age-depth chart in Extended Data Fig. 1, and tie points of Age Model 1 used for linear extrapolation of environmental proxies in Supplementary Data Table 3. Four age models were explored; Model One is preferred. Model One and Model Two minimise inconsistency with biostratigraphic first occurrences, place the E-O boundary at 547 mbsf, and assign the interval of normal polarity between 435 and 503 mbsf to Chron C13n. Model One and Model Two place different priority on inconsistencies with biostratigraphic last occurrences, and the robustness of intervals of magnetic reversals constrained by only a few observations. Model One minimises inconsistencies with the geomagnetic polarity record, but does not seek to minimise biostratigraphic last occurrences. In contrast, Model Two requires that the intervals of normal polarity at

408 m and 421 mbsf, constrained by only one and two measurements of magnetic polarity respectively[59], are a transient, local signal not reflective of the global magnetic field. Models Three and Four explore the possibility that the interval of normal polarity between 435 and 503 mbsf is Chron C15n (Model Three) or Chron C12n (Model Four). Model Three is the most unlikely, as it contains seven inconsistencies with biostratigraphic first occurrences across four fossil groups. Model Four is consistent with the paleomagnetic record, and the biostratigraphic first occurrences, but is inconsistent with every available biostratigraphic last occurrence. It would also require a pronounced increase in the proportion of protoperidinioid dinoflagellates cysts observed between 495 and 530 mbsf to have occurred more than 2 million years later than observed in other circum-Antarctic cores[62].

One perplexing aspect of the CIROS-1 biostratigraphy is the virtual absence of the dinoflagellate cyst *Malvinia escutiana*, which has a first occurrence in the earliest Oligocene in other Southern Ocean records[61]. A single specimen of *M. escutiana* was recorded in CIROS-1, at 376.39 mbsf, within Subchron C11n.2n of age Model One (this study). *M. escutiana* has been identified in the nearby CRP-3 core[62]. Those authors do not report their count data for their CRP-3 dinoflagellates cysts, but note that specimens of *M. escutiana* were recorded somewhere in the interval between 13.4 and 151.97 mbsf. Following the age model for CRP-3 (Age Model 3[67]), this would place the CRP-3 occurrences of *M. escutiana* within Chron C12n to upper C12r. This suggests *M. escutiana* may not have a significant presence in the Ross Sea in the earliest Oligocene, in contrast to observations on the Wilkes Land margin at IODP Site U1356[52,62].

371 **DSDP 270**

372 Deep Sea Drilling Project Site 270 was recovered from the Eastern Basin of the central Ross Sea in
373 1973 (Fig. 1)[68] (The Shipboard Scientific Party, 1975a). This core records a deepening sequence of
374 glacimarine sediments, represented by glacimarine mudstones, interstratified mudstones and sandstones,
375 and massive and stratified diamictites[34,42,68]. Samples for this study have been taken from glacimarine
376 sediments between 387.9 and 27.8 mbsf, dated as late Oligocene to early Miocene[42].

377 **CRP 2/2A**

378 The Cape Roberts Project recovered CRP 2/2A off the Victoria Land coast of Antarctica in 1999 (Fig.
379 1)[35]. Samples have been taken from three glacimarine sediment sequences in the upper Oligocene/lower
380 Miocene section of the core, recording the expansion and contraction of the East Antarctic Ice Sheet
381 (EAIS)[69,70].

382 **ANDRILL-2A**

383 The AND-2A core was recovered in 2007 from Southern McMurdo Sound as part of the ANDRILL
384 program (Fig. 1)[11]. Samples for this compilation were collected from the lower Miocene to mid-
385 Miocene section of the core, and were published as TEX_{86}^{L} values[11], calibrated to Kim et al. (2012)[71]
386 (Supplementary Data Table 4). Glacimarine sediments through this section represent ice-distal to ice-
387 proximal, and occasionally subglacial settings, reflecting advance and retreat of grounded ice across the
388 drill site[72,73].

DSDP 274

DSDP Site 274 was drilled on the lower continental rise in the northwestern Ross Sea in 1973 (Fig. 1)[68]. Samples for this study were taken from middle Miocene diatom-rich silty clay at 156-142 mbsf. Ages have been assigned using the relaxed hybrid CONOP model of Crampton et al. (2016)[74] (Supplementary Data Table 3). This model does not extend below 141.26 mbsf. For samples below this depth, the same linear sedimentation rate that occurs above 141.26 mbsf is used. This is constrained by the first appearance of *Denticulopsis maccollumii* at 141.26 mbsf (dated to 17.05 Ma) and the first appearance of *Actinocyclus ingens* at 113.6 mbsf (dated to 15.83 Ma). The continuation of this sedimentation rate is supported by the apparent lack of a hiatus or change in lithology through this interval[68].

ANDRILL-1B

The AND-IB core was drilled in 2006 as part of the ANDRILL McMurdo Ice Shelf Project (Fig. 1), and samples were compiled from published data from the Plio-Pleistocene section of the core[1] (Supplementary Data Table 4). Pliocene sediments reflect successions of advance and retreat of the marine-based ice sheet in the Ross Sea, and consist of cycles of diamictite, mudstone and diatomite, bounded by glacial erosion surfaces[26].

GDGT processing and analysis

Samples from DSDP 270, CRP-2/2A and DSDP 274 were processed for glycerol dialkyl glycerol tetraethers at the Birmingham Molecular Climatology Laboratory, University of Birmingham. Lipids were extracted from ~10-15 g of homogenised sediment by ultrasonic extraction using dichloromethane

(DCM):methanol (3:1). The total lipid extract was fractionated by silica gel chromatography using n-hexane, n-hexane:DCM (2:1), DCM, and methanol to produce four separate fractions, the last of which contained the GDGTs. Procedural blanks were also analysed to ensure the absence of laboratory contaminants.

Samples were filtered using hexane:isopropanol (99:1) through a 0.4 μm PTFE filter (Alltech part 2395), before being dried under a continuous stream of N_2. Samples were then sent to Yale University for analysis. Samples were redissolved in hexane:isopropanol (99:1), and analysed and quantified on an Agilent single quadrupole Liquid Chromatography/Mass Spectrometer (LC-MS) 6100 series using previously established protocols[75]. Due to frequent low abundances of compounds, some samples were re-run at higher concentrations, and integrations derived from these re-runs were favoured. Samples were integrated multiple times and averaged to account for potential integration variation, with an average TEX_{86} standard deviation of 0.007 between integrations. The areas of individual GDGTs, as well as calculated indices and temperature calibrations are recorded in supplementary Data Table 4.

Methodology for samples from AND-1B and AND-2A are described in previous works[11,26]. Unpublished results for samples from CIROS-1 and the McMurdo Erratics were processed and analysed at NIOZ using methods outlined in Schouten et al. (2007). A further 4 previously unpublished results for samples from DSDP 274 (depths 153.63 mbsf, 155.68 mbsf, 163.75 mbsf, 174.2 mbsf) were also added to the compilation. These were extracted using an accelerated solvent extractor, then fractionated by Al_2O_3 column chromatography using hexane:DCM (9:1, v:v), hexane:DCM (1:1) and DCM:MeOH

(1:1). The samples were then dissolved in hexane:isopropanol (99:1, v/v) and filtered over a 0.45-μm polytetrafluoroethylene filter, before being analysed following procedures outlined in Hopmans et al. (2016). As samples were processed at three different laboratory facilities (University of Birmingham, Yale University and NIOZ), and analysed between two facilities (Yale University and NIOZ), the potential for interlaboratory biases must be considered. Previously reported results from a comparison of 35 laboratories and found that TEX_{86} and BIT indices were not significantly affected by differences in sediment extraction and processing techniques[76]. TEX_{86} measurements had an interlaboratory reproducibility for different samples ranging from 0.023 to 0.053, with the differences suggested to be due to instrumental characteristics. The BIT index was found to have good reproducibility at the extremes of the index, where values were close to either 0 or 1, but poorer reproducibility for intermediate values with values typically overestimated. Samples from AND-1B were processed and analysed at both Yale University and NIOZ. Chromatograms of samples analysed in each laboratory were integrated by members of the other for comparison and were found to have an average SST difference of ±0.8°C, when the TEX_{86}^{L} calibration[77] was used[26]. Four samples processed at Yale University were also analysed at NIOZ with an average SST difference of 0.8°C[26]. The results discussed above suggest that while some interlaboratory differences are possible, they are likely to have a minor influence on reported SST values[26,76].

CO_2 compilation.

The compilation of atmospheric CO_2 concentrations, is based off previous compilations[47,78,79], but updated with more recent datasets[47,79,79–85]. One outlier value of 2622 ppm has been removed at 36.48

Ma. Moving averages for CO_2 and temperature datasets were been derived using 'mwStats' in the R-package 'astrochron'[86].

Ice sheet model

Modelling sensitivity tests have previously demonstrated large ice volume differences can result solely from changing topographic boundary conditions through time[8,39,40,87]. To assess the potential impact topographic changes between the EOT and OMT may have had on oxygen isotope shifts in deep sea records, here we expanded on previous ice sheet modelling experiments of Paxman et al., (2020)[8] by rerunning selected experiments with an isotope enabled ice sheet model[88]. Experiments run under a steady state climate with an atmospheric CO_2 concentration of 500 ppm and an imposed 5°C warming of the ocean relative to present show a larger AIS (34.6 $x10^6$ km^3) was in place with an EOT topography relative to experiments with the same climate and an OMT topography, which had a greatly reduced ice volume (28.9 $x10^6$ km^3), with most of this change occurring in the WAIS. Our isotope enabled simulations suggest that solely due to changes in topography, there would have been a shift in the oxygen isotope composition of seawater of 0.2 ‰. These experiments did not include the Marine Ice Cliff Instability (MICI)[41] and were chosen as they demonstrated the greatest sensitivity to topographic change with the chosen climate forcing. Although beyond the scope of this study we expect that at a lower atmospheric CO_2 forcing and ocean warming there would be comparable (or greater) sensitivity to changes to topography in experiments including MICI.

References

1. Naish, T. *et al*. Obliquity-paced Pliocene West Antarctic ice sheet oscillations. *Nature* **458**, 322–328 (2009).
2. Palike, H. *et al*. The Heartbeat of the Oligocene Climate System. *Science* **314**, 1894–1898 (2006).
3. Westerhold, T. *et al*. An astronomically dated record of Earth's climate and its predictability over the last 66 million years. *Science* **369**, 1383–1387 (2020).
4. Naish, T. R. *et al*. Orbitally induced oscillations in the East Antarctic ice sheet at the Oligocene/Miocene boundary. *Nature* **413**, 719–723 (2001).
5. Rae, J. W. B. *et al*. Atmospheric CO_2 over the Past 66 Million Years from Marine Archives. *Annu*. *Rev*. *Earth Planet*. *Sci*. **49**, 609–641 (2021).
6. Kennett, J. P. *et al*. Development of the Circum-Antarctic Current. *Science* **186**, 144–147 (1974).
7. Wilson, D. S. & Luyendyk, B. P. West Antarctic paleotopography estimated at the Eocene-Oligocene climate transition. *Geophys*. *Res*. *Lett*. **36**, 4 PP. (2009).
8. Paxman, G. J. G., Gasson, E. G. W., Jamieson, S. S. R., Bentley, M. J. & Ferraccioli, F. Long-Term Increase in Antarctic Ice Sheet Vulnerability Driven by Bed Topography Evolution. *Geophysical Research Letters* **47**, e2020GL090003 (2020).
9. Zachos, J., Pagani, M., Sloan, L., Thomas, E. & Billups, K. Trends, Rhythms, and Aberrations in Global Climate 65 Ma to Present. *Science* **292**, 686–693 (2001).
10. Pollard, D. & DeConto, R. M. Modelling West Antarctic ice sheet growth and collapse through the past five million years. *Nature* **458**, 329–332 (2009).
11. Levy, R. *et al*. Antarctic ice sheet sensitivity to atmospheric CO_2 variations in the early to mid-Miocene. *Proceedings of the National Academy of Sciences of the United States of America* **113**, 3453–3458 (2016).
12. Gomez, N., Weber, M. E., Clark, P. U., Mitrovica, J. X. & Han, H. K. Antarctic ice dynamics amplified by Northern Hemisphere sea-level forcing. *Nature* **587**, 600–604 (2020).
13. Sorlien, C. C. *et al*. Oligocene development of the West Antarctic Ice Sheet recorded in eastern Ross Sea strata. *Geology* **35**, 467–470 (2007).

14. Paxman, G. J. G. *et al*. Reconstructions of Antarctic topography since the Eocene–Oligocene boundary. *Palaeogeography, Palaeoclimatology, Palaeoecology* **535**, 109346 (2019).
15. De Santis, L., Anderson, J. B., Brancolini, G. & Zayatz, I. Seismic Record of Late Oligocene Through Miocene Glaciation on the Central and Eastern Continental Shelf of the Ross Sea. in *Geology and Seismic Stratigraphy of the Antarctic Margin* (eds. Cooper, A. K., Barker, P. F. & Brancolini, G.) 235–260 (American Geophysical Union, 1995).
16. Schouten, S., Hopmans, E. C. & Sinninghe Damsté, J. S. The organic geochemistry of glycerol dialkyl glycerol tetraether lipids: A review. *Organic Geochemistry* **54**, 19–61 (2013).
17. Dunkley Jones, T. *et al*. OPTiMAL: a new machine learning approach for GDGT-based palaeothermometry. *Climate of the Past* **16**, 2599–2617 (2020).
18. Hartman, J. D. *et al*. Paleoceanography and ice sheet variability offshore Wilkes Land, Antarctica – Part 3: Insights from Oligocene–Miocene TEX_{86}-based sea surface temperature reconstructions. *Climate of the Past* **14**, 1275–1297 (2018).
19. Sangiorgi, F. *et al*. Southern Ocean warming and Wilkes Land ice sheet retreat during the mid-Miocene. *Nature Communications* **9**, 317 (2018).
20. Stilwell, J. D. & Feldmann, R. M. *Paleobiology and Paleoenvironments of Eocene Rocks: McMurdo Sound, East Antarctica*. (American Geophysical Union, 2000).
21. Galeotti, S. *et al*. Antarctic Ice Sheet variability across the Eocene-Oligocene boundary climate transition. *Science* **352**, 76–80 (2016).
22. Carter, A., Riley, T. R., Hillenbrand, C.-D. & Rittner, M. Widespread Antarctic glaciation during the Late Eocene. *Earth and Planetary Science Letters* **458**, 49–57 (2017).
23. Liu, Z. *et al*. Global Cooling During the Eocene-Oligocene Climate Transition. *Science* **323**, 1187–1190 (2009).
24. Feakins, S. J., Warny, S. & Lee, J.-E. Hydrologic cycling over Antarctica during the middle Miocene warming. *Nature Geosci* **5**, 557–560 (2012).
25. Lewis, A. R. & Ashworth, A. C. An early to middle Miocene record of ice-sheet and landscape evolution from the Friis Hills, Antarctica. *GSA Bulletin* **128**, 719–738 (2016).
26. McKay, R. *et al*. Antarctic and Southern Ocean influences on Late Pliocene global cooling. *PNAS* **109**, 6423–6428 (2012).

27. Haywood, A. M. *et al*. Large-scale features of Pliocene climate: results from the Pliocene Model Intercomparison Project. *Clim*. *Past* **9**, 191–209 (2013).
28. Cramer, B. S., Toggweiler, J. R., Wright, J. D., Katz, M. E. & Miller, K. G. Ocean overturning since the late cretaceous: Inferences from a new benthic foraminiferal isotope compilation. *Paleoceanography* **24**, (2009).
29. Miller, K. G. *et al*. Cenozoic sea-level and cryospheric evolution from deep-sea geochemical and continental margin records. *Science Advances* **6**, eaaz1346 (2020).
30. Villa, G., Fioroni, C., Persico, D., Roberts, A. P. & Florindo, F. Middle Eocene to Late Oligocene Antarctic glaciation/deglaciation and Southern Ocean productivity. *Paleoceanography* **29**, 223–237 (2014).
31. Hoem, F. S. *et al*. Temperate Oligocene surface ocean conditions offshore of Cape Adare, Ross Sea, Antarctica. *Climate of the Past* **17**, 1423–1442 (2021).
32. Bijl, P. K. *et al*. Paleoceanography and ice sheet variability offshore Wilkes Land, Antarctica – Part 2: Insights from Oligocene–Miocene dinoflagellate cyst assemblages. *Climate of the Past* **14**, 1015–1033 (2018).
33. Salabarnada, A. *et al*. Paleoceanography and ice sheet variability offshore Wilkes Land, Antarctica - Part 1: Insights from late Oligocene astronomically paced contourite sedimentation. *Climate of the Past* **14**, 991–1014 (2018).
34. Leckie, R. M. & Webb, P.-N. Late Oligocene–early Miocene glacial record of the Ross Sea, Antarctica: Evidence from DSDP Site 270. *Geology* **11**, 578–582 (1983).
35. Barrett, P. J. Cenozoic Climate and Sea Level History from Glacimarine Strata off the Victoria Land Coast, Cape Roberts Project, Antarctica. in *Glacial Sedimentary Processes and Products* (eds. Hambrey, M. J., Christoffersen, P., Glasser, N. F. & Hubbard, B.) 259–287 (Blackwell Publishing Ltd., 2007).
36. Pekar, S. F., DeConto, R. M. & Harwood, D. M. Resolving a late Oligocene conundrum: Deep-sea warming and Antarctic glaciation. *Palaeogeography, Palaeoclimatology, Palaeoecology* **231**, 29–40 (2006).
37. Hauptvogel, D. W., Pekar, S. F. & Pincay, V. Evidence for a heavily glaciated Antarctica during the late Oligocene "warming" (27.8–24.5 Ma): Stable isotope records from ODP Site 690. *Paleoceanography* **32**, 384–396 (2017).
38. O'Brien, C. L. *et al*. The enigma of Oligocene climate and global surface temperature evolution. *PNAS* **117**, 25302–25309 (2020).

39. Gasson, E., DeConto, R. M., Pollard, D. & Levy, R. H. Dynamic Antarctic ice sheet during the early to mid-Miocene. *PNAS* **113**, 3459–3464 (2016).
40. Colleoni, F. *et al*. Past continental shelf evolution increased Antarctic ice sheet sensitivity to climatic conditions. *Sci Rep* **8**, (2018).
41. DeConto, R. M. & Pollard, D. Contribution of Antarctica to past and future sea-level rise. *Nature* **531**, 591–597 (2016).
42. Kulhanek, D. K. *et al*. Revised chronostratigraphy of DSDP Site 270 and late Oligocene to early Miocene paleoecology of the Ross Sea sector of Antarctica. *Global and Planetary Change* **178**, 46–64 (2019).
43. Marschalek, J. W. *et al*. A large West Antarctic Ice Sheet explains early Neogene sea-level amplitude. *Nature* **600**, 450–455 (2021).
44. Hill, D. J., Bolton, K. P. & Haywood, A. M. Modelled ocean changes at the Plio-Pleistocene transition driven by Antarctic ice advance. *Nature Communications* **8**, 14376 (2017).
45. Levy, R. H. *et al*. Antarctic ice-sheet sensitivity to obliquity forcing enhanced through ocean connections. *Nature Geoscience* **12**, 132–137 (2019).
46. Foster, G. L., Royer, D. L. & Lunt, D. J. Future climate forcing potentially without precedent in the last 420 million years. *Nature Communications* **8**, 14845 (2017).
47. Greenop, R. *et al*. Orbital Forcing, Ice Volume, and CO_2 Across the Oligocene-Miocene Transition. *Paleoceanography and Paleoclimatology* **34**, 316–328 (2019).
48. Locarnini, M. M. *et al*. World ocean atlas 2018, volume 1: Temperature. (2018).
49. Orsi, A. H., Whitworth, T. & Nowlin, W. D. On the meridional extent and fronts of the Antarctic Circumpolar Current. *Deep Sea Research Part I: Oceanographic Research Papers* **42**, 641–673 (1995).
50. Liebrand, D. *et al*. Cyclostratigraphy and eccentricity tuning of the early Oligocene through early Miocene (30.1–17.1 Ma): Cibicides mundulus stable oxygen and carbon isotope records from Walvis Ridge Site 1264. *Earth and Planetary Science Letters* **450**, 392–405 (2016).
51. Haslett, J. & Parnell, A. A simple monotone process with application to radiocarbon-dated depth chronologies. *Journal of the Royal Statistical Society: Series C (Applied Statistics)* **57**, 399–418 (2008).

570 52. Bijl, P. K., Houben, A. J. P., Bruls, A., Pross, J. & Sangiorgi, F. Stratigraphic calibration of Oligocene-Miocene organic-
571 walled dinoflagellate cysts from offshore Wilkes Land, East Antarctica, and a zonation proposal. *Journal of*
572 *Micropalaeontology* **37**, 105–138 (2018).
573 53. Harwood, D. M. & Levy, R. H. The McMurdo Erratics: Introduction and Overview. in *Paleobiology and*
574 *Paleoenvironments of Eocene Rocks: McMurdo Sound, East Antarctica* (eds. Stilwel, J. D. & Feldman, R. M.) 1–18
575 (American Geophysical Union, 2000).
576 54. Barrett, P. J. Antarctic Cenozoic History From CIROS-1 Drill Hole, McMurdo Sound, DSIR Bulletin 245. *Antarctic*
577 *Cenozoic History from the CIROS-1 Drillhole, McMurdo Sound* (1989).
578 55. Hambrey, M. J., Barrett, P. J. & Robinson, P. H. Stratigraphy. *Antarctic Cenozoic History from the CIROS-1 drillhole,*
579 *McMurdo Sound* **245**, 23–48 (1989).
580 56. Roberts, A. P., Wilson, G. S., Harwood, D. M. & Verosub, K. L. Glaciation across the Oligocene-Miocene boundary in
581 southern McMurdo Sound, Antarctica: New chronology from the CIROS-1 drill hole. *Palaeogeography,*
582 *Palaeoclimatology, Palaeoecology* **198**, 113–130 (2003).
583 57. Coccioni, R. & Galeotti, S. Foraminiferal Biostratigraphy and Palaeoecology of the CIROS-1 Core from McMurdo Sound
584 (Ross Sea, Antarctica). *Terra Antarctica* **4**, 103–117 (1997).
585 58. Hannah, M. J. Climate Controlled Dinoflagellate Distribution in Late Eocene - Earliest Oligocene Strata from CIROS-1
586 Drillhole, McMurdo Sound, Antarctica. *Terra Antarctica* **4**, 73–78 (1997).
587 59. Wilson, G. S., Roberts, A. P., Verosub, K. L., Florindo, F. & Sagnotti, L. Magnetobiostratigraphic chronology of the
588 Eocene-Oligocene transition in the CIROS-1 core, Victoria Land margin, Antarctica: Implications for Antarctic glacial
589 history. *Bulletin of the Geological Society of America* **110**, 35–47 (1998).
590 60. Clowes, C. D., Hannah, M. J., Wilson, G. J. & Wrenn, J. H. Marine palynostratigraphy and new species from the Cape
591 Roberts drill-holes, Victoria land basin, Antarctica. *Marine Micropaleontology* **126**, 65–84 (2016).
592 61. Houben, A. J. P., Bijl, P. K., Guerstein, G. R., Sluijs, A. & Brinkhuis, H. Malvinia escutiana, a new biostratigraphically
593 important Oligocene dinoflagellate cyst from the Southern Ocean. *Review of Palaeobotany and Palynology* **165**, 175–182
594 (2011).

595 62. Houben, A. J. P. *et al*. Reorganization of Southern Ocean plankton ecosystem at the onset of Antarctic glaciation. *Science*
596 **340**, 341–344 (2013).
597 63. Ogg, J. G. Chapter 5 - Geomagnetic Polarity Time Scale. in *The Geologic Time Scale* (eds. Gradstein, F. M., Ogg, J. G.,
598 Schmitz, M. D. & Ogg, G. M.) 85–113 (Elsevier, 2012). doi:10.1016/B978-0-444-59425-9.00005-6.
599 64. Prebble, J. G., Raine, J. I., Barrett, P. J. & Hannah, M. J. Vegetation and climate from two Oligocene glacioeustatic
600 sedimentary cycles (31 and 24 Ma) cored by the Cape Roberts Project, Victoria Land Basin, Antarctica. *Palaeogeography,*
601 *Palaeoclimatology, Palaeoecology* **231**, 41–57 (2006).
602 65. Truswell, E. M. & Drewry, D. J. Distribution and provenance of recycled palynomorphs in surficial sediments of the Ross
603 Sea, Antarctica. *Marine Geology* **59**, 187–214 (1984).
604 66. Watkins, D. K., Wise, S. W. & Villa, G. Calcareous nannofossils from Cape Roberts Project drillhole CRP-3, Victoria
605 Land Basin, Antarctica. *Terra Antarctica* **8**, 339–346 (2001).
606 67. Galeotti, S. *et al*. Cyclochronology of the Eocene-Oligocene transition from the Cape Roberts Project-3 core, Victoria
607 Land basin, Antarctica. *Palaeogeography, Palaeoclimatology, Palaeoecology* **335–336**, 84–94 (2012).
608 68. Hayes, D. E., Frakes, L. A., & et al. *Initial Reports of the Deep Sea Drilling Project, 28*. vol. 28 (U.S. Government Printing
609 Office, 1975).
610 69. Florindo, F., Wilson, G. S., Roberts, A. P., Sagnotti, L. & Verosub, K. L. Magnetostratigraphic chronology of a late
611 Eocene to early Miocene glacimarine succession from the Victoria Land Basin, Ross Sea, Antarctica. *Global and*
612 *Planetary Change* **45**, 207–236 (2005).
613 70. Naish, T. R., Wilson, G. S., Dunbar, G. B. & Barrett, P. J. Constraining the amplitude of Late Oligocene bathymetric
614 changes in western Ross Sea during orbitally-induced oscillations in the East Antarctic Ice Sheet: (2) Implications for
615 global sea-level changes. *Palaeogeography, Palaeoclimatology, Palaeoecology* **260**, 66–76 (2008).
616 71. Kim, J.-H. *et al*. Holocene subsurface temperature variability in the eastern Antarctic continental margin. *Geophys. Res.*
617 *Lett*. **39**, L06705 (2012).

72. Fielding, C. R. *et al*. Sequence stratigraphy of the ANDRILL AND-2A drillcore, Antarctica: A long-term, ice-proximal record of Early to Mid-Miocene climate, sea-level and glacial dynamism. *Palaeogeography, Palaeoclimatology, Palaeoecology* **305**, 337–351 (2011).

73. Passchier, S. *et al*. Early and middle Miocene Antarctic glacial history from the sedimentary facies distribution in the AND-2A drill hole, Ross Sea, Antarctica. *Geological Society of America Bulletin* B30334.1 (2011) doi:10.1130/B30334.1.

74. Crampton, J. S. *et al*. Southern Ocean phytoplankton turnover in response to stepwise Antarctic cooling over the past 15 million years. *Proceedings of the National Academy of Sciences of the United States of America* **113**, 6868–6873 (2016).

75. Schouten, S., Huguet, C., Hopmans, E. C., Kienhuis, M. V. M. & Sinninghe Damsté, J. S. Analytical methodology for TEX86 paleothermometry by high-performance liquid chromatography/atmospheric pressure chemical ionization-mass spectrometry. *Analytical Chemistry* **79**, 2940–2944 (2007).

76. Schouten, S. *et al*. An interlaboratory study of TEX86 and BIT analysis of sediments, extracts, and standard mixtures. *Geochemistry, Geophysics, Geosystems* **14**, 5263–5285 (2013).

77. Kim, J.-H. *et al*. New indices and calibrations derived from the distribution of crenarchaeal isoprenoid tetraether lipids: Implications for past sea surface temperature reconstructions. *Geochimica et Cosmochimica Acta* **74**, 4639–4654 (2010).

78. Masson-Delmotte, V. *et al*. Information from paleoclimate archives. *Climate change* 383–464 (2013).

79. Sosdian, S. M. *et al*. Constraining the evolution of Neogene ocean carbonate chemistry using the boron isotope pH proxy. *Earth and Planetary Science Letters* **498**, 362–376 (2018).

80. Martínez-Botí, M. A. *et al*. Plio-Pleistocene climate sensitivity evaluated using high-resolution CO2 records. *Nature* **518**, 49–54 (2015).

81. Greenop, R., Foster, G. L., Wilson, P. A. & Lear, C. H. Middle Miocene climate instability associated with high-amplitude CO2 variability. *Paleoceanography* **29**, 845–853 (2014).

82. Badger, M. P. S. *et al*. Insensitivity of alkenone carbon isotopes to atmospheric CO_2 at low to moderate CO_2 levels. *Climate of the Past* **15**, 539–554 (2019).

642 83. Mejía, L. M. *et al*. A diatom record of CO2 decline since the late Miocene. *Earth and Planetary Science Letters* **479**, 18–
643 33 (2017).
644 84. Super, J. R. *et al*. North Atlantic temperature and pCO2 coupling in the early-middle Miocene. *Geology* **46**, 519–522
645 (2018).
646 85. Witkowski, C. R., Weijers, J. W. H., Blais, B., Schouten, S. & Damsté, J. S. S. Molecular fossils from phytoplankton
647 reveal secular Pco2 trend over the Phanerozoic. *Science Advances* (2018) doi:10.1126/sciadv.aat4556.
648 86. Meyers, S., Malinverno, A., Hinnov, L., Zeeden, C. & Moron, V. *astrochron: A Computational Tool for Astrochronology*.
649 (2019).
650 87. Wilson, D. S., Pollard, D., DeConto, R. M., Jamieson, S. S. R. & Luyendyk, B. P. Initiation of the West Antarctic Ice
651 Sheet and estimates of total Antarctic ice volume in the earliest Oligocene. *Geophys*. *Res*. *Lett*. **40**, 4305–4309 (2013).
652 88. DeConto, R. M. *et al*. Thresholds for Cenozoic bipolar glaciation. *Nature* **455**, 652–656 (2008).

653
654

655 **Corresponding Author:** Correspondence should be addressed to Dr Bella Duncan
656 (Bella.Duncan@vuw.ac.nz).

657

658 **Acknowledgements**

659 The authors thank the anonymous reviewers for their helpful feedback which has much improved the
660 paper. We are grateful for access to samples from the IODP core repository at Texas A&M University
661 for DSDP Sites 270 and 274, and to the Alfred Wegener Institute for access to samples from the Cape
662 Roberts Project. This study was funded via an Antarctica New Zealand Sir Robin Irvine PhD
663 Scholarship and Scientific Committee of Antarctic Research Fellowship awarded to B. Duncan, with
664 additional funding by the Royal Society Te Apārangi Marsden Fund award MFP-VUW1808, and the

New Zealand Ministry of Business Innovation and Employment through the Antarctic Science Platform (ANTA1801), and Contract C05X1001. The Natural Environment Research Council funded J. Bendle (Standard Grant Ne/I00646X/1). D. Kulhanek was supported by US National Science Foundation award OCE-1326927. The authors are grateful for support from IODP and support in kind from the University of Birmingham and Yale University. We thank Stefan Schouten (NIOZ) for laboratory support and assistance with temperature data, and James Super for assistance with sample analysis while at Yale University.

Author contributions

B.D, R.M., J.B., R.L. and T.N. designed the research. B.D. processed samples for DSDP 270, DSDP 274 and CRP-2/2A. S.K. conducted analysis on DSDP 270, DSDP 274 and CRP-2/2A. F.S. processed samples and conducted analysis on AND-2A. F.H. processed samples and conducted analysis on additional samples for DSDP 274. V.W. processed samples and conducted analysis on AND-1B, CIROS-1 and the McMurdo Erratics. C.W. processed samples and conducted analysis on AND-1B. J.P. and C.C. developed the age model for CIROS-1. S.M. contributed statistical analyses. E.G. provided ice volume model output and advised on interpretation. T.D.J. assisted with temperature calibration interpretations. D.K.K. and C.K. assisted with sedimentological and environmental interpretations for DSDP 270. H.M. advised on laboratory processing and data interpretation. G.T.V. advised on GDGT data interpretation. B.D. created the figures and wrote the text with assistance from all authors, in particular R.M., J.B., R.L. and T.N.

Data Availability

Data sets generated during and/or analysed during the current study are available in Supplementary Data Tables 1-4.

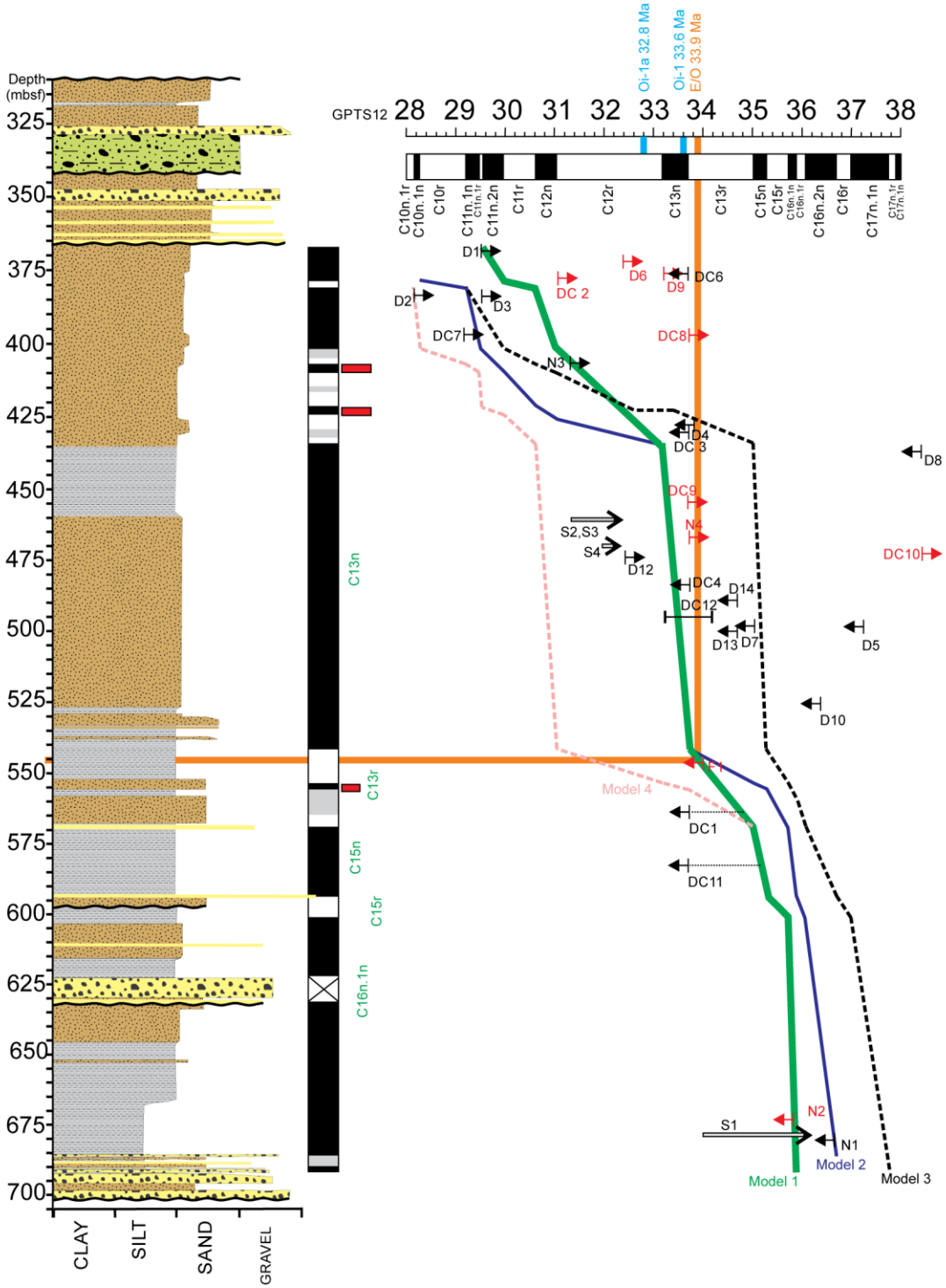

Extended Data Figure 1. Age model for CIROS-1, based on the paleo-magnetic record from Wilson et al. (1998) and new biostratigraphic events described in Supplementary Data Table 1. The preferred age model is shown in green (model 1), as described in Methods section.